Proton Transport through Influenza A Virus M2 Protein Reconstituted in Vesicles

J. Craig Moffat,* Viksita Vijayvergiya,* Philip F. Gao,† Timothy A. Cross,† Dixon J. Woodbury,* and David D. Busath*

*Department of Physiology and Developmental Biology, Brigham Young University, Provo, Utah; and †Department of Chemistry and Biochemistry, National High Magnetic Field Laboratory, Florida State University, Tallahassee, Florida

ABSTRACT Influenza A virus M2 protein is known to form acid-activated, proton-selective, amantadine-sensitive channels. We directly measured proton uptake in vesicles containing reconstituted M2 by monitoring external pH after addition of valinomycin to vesicles with 100-fold-diluted external [K^+]. External pH typically increased by a few tenths of a pH unit over a few minutes after valinomycin addition, but proton uptake was not significantly altered by acidification. Under neutral conditions, external addition of 1 mM amantadine produced a reduction in flux consistent with randomly ordered channels; however, experimental variation is high with this method and the block was not statistically significant. Amantadine block was reduced at pH 5.4. In accord with Lin and Schroeder's study of reconstituted M2 using a pH-sensitive dye to monitor intravesicular pH, we conclude that bath pH weakly affects or does not significantly affect proton flow in the pH range 5.4–7.0 for the reconstituted system, contrary to results from electrophysiological studies. Theoretical analysis of the relaxation to Donnan equilibrium utilized for such vesicle uptake assays illuminates the appropriate timescale of the initial slope and an important limitation that must be placed on inferences about channel ion selectivity. The rise in pH over 10 s after ionophore addition yielded time-averaged single-channel conductances of 0.35 ± 0.20 aS and 0.72 ± 0.42 aS at pH 5.4 and 7.0, respectively, an order of magnitude lower than previously reported in vesicles. Assuming complete membrane incorporation and tetramerization of the reconstituted protein, such a low time-averaged conductance in the face of previously observed single-channel conductance (6 pS at pH 3) implies an open channel probability of 10^{-6}–10^{-4}. Based on leakage of potassium from M2-containing vesicles, compared to protein-free vesicles, we conclude that M2 exhibits $\sim 10^7$ selectivity for hydrogen over potassium.

INTRODUCTION

The influenza virus M2 protein, target of the antiviral drugs amantadine and rimantadine, forms an acid-activated proton-conducting ion channel which functions during viral uncoating and maturation by modifying the pH in virions as well as in trans-Golgi vesicles (1,2). The M2 channel is known to be highly selective for protons and has low permeability for other physiological ions according to reversal potential studies (3). The ion channel activity has been observed in whole cell *Xenopus* oocytes, mammalian cells, and yeast cells (4–7) and in planar lipid bilayers (8). This protein is a homotetramer of 97 amino acid residues (9,10) with 23 amino acids of the N-terminus oriented extracellularly, a single internal hydrophobic domain of 19 residues that acts as the transmembrane domain and forms the pore of the channel, and a 54-residue cytoplasmic tail. Histidine-37 (His-37), within the transmembrane domain, has been implicated in the activation and proton selectivity of the channel and may be involved in proton translocation (7). Tryptophan-41 (Trp-41) has been shown to influence the pH-dependent characteristics of the channel (11).

The shape of the channel has been well characterized. M2 is a symmetric or pseudosymmetric tetramer (12) with the membrane-spanning region being a left-handed coiled coil (13,14). The helices are separated by 8 Å and the Trp-41 on the i^{th} helix and His-37 of the i^{th} + 1 helix are paired, since they are separated by only 3.9 Å (15). The helical tilt pivots near His-37 and is flexible to allow the membrane-spanning region to fit within the bilayer thickness (16). This accounts for the variety of tilt angles from the bilayer normal of 15°–38° reported in a variety of lipid systems (13,16–19). Using hydrogen/deuterium exchange with the whole protein, Tian et al. (20) showed the presence of an aqueous pore. These data support the notion that M2 homotetramers form an ion conduction pathway.

The mechanisms of selective M2 proton conductivity (21) and pH activation (22) are matters of current debate. Two main selective conductivity mechanisms have been suggested: gated Grotthus conductance (23,24) and shuttling (25). In the gated Grotthus mechanism, conductivity is achieved when water molecules are able to penetrate the channel throughout, forming a continuous, conductive proton wire. In the shuttling

Submitted March 22, 2007, and accepted for publication August 13, 2007.

Address reprint requests to David D. Busath, Dept. of Physiology and Developmental Biology, Brigham Young University, 574 Widtsoe Building, Provo, UT 84602. Tel.: 801-422-8753; Fax: 801-422-0700; E-mail: david_busath@byu.edu.

J. Craig Moffat's present address is Dean's Office, School of Medicine, University of Utah, Salt Lake City, Utah.

Viksita Vijayvergiya's present address is Dept. of Pharmacology and Physiology, School of Medicine and Dentistry, University of Rochester, Rochester, NY 14642.

Editor: Peter C. Jordan.

0006-3495/08/01/434/12 $2.00

doi: 10.1529/biophysj.107.109082

mechanism, the histidines are directly involved in the proton transfer mechanism. A biprotonated histidine intermediate is transiently formed, leading to rapid proton release at the opposite side of the histidine ring. Regeneration occurs through tautomerization or flipping of the imidazole ring. Lear (26) presented a detailed kinetic analysis of the M2 current, which is designed to apply to the shuttle mechanism but could also apply to the gated Grotthus mechanism if a saturable serially accessible proton binding site exists in the channel. Smondyrev and Voth (27) provided the first simulation evidence for the gated Grotthus conductance mechanism via a molecular dynamics simulation methodology that was capable of describing explicit proton transport by the Grotthus mechanism. Details of the protein structure and dynamics underlying selective proton transport are still far from settled.

Conceptually, one would expect the term ''acid activation'' to refer to increased flux protons at lower pH, above and beyond what one would expect from mass action (28) modified by saturation (3); or to increased probability of the open state (P_o) for single channels. Although proton current does go up by 2- to10-fold as pH is reduced by 1.5–2 pH units (2,3,5,28–31), the increase is generally an order of magnitude lower than expected from mass action, let alone with acid-gating in addition to mass-action. The increase is even lower in the one previously reported reconstitution experiment (32), where a pH change of 1.4 pH units induced only a twofold increase in vesicle proton uptake. These sub-mass-action increases could be due to saturation of an obligatory site in the proton transport pathway. Clear experimental evidence of acid-activation can be observed when extracellular fluid is basified: whole-cell outward M2 current is decreased, even though the driving force on protons is increased (3). For reconstituted M2, where single-channel currents have been observed, single-channel currents increase with decreasing pH, as expected from mass action (modulated by saturation (8)), but P_o changes have not been determined, so no evidence of acid-gating is yet available at the single-channel level.

Proton translocation into vesicles with reconstituted M2 proteins has been measured previously using an intravesicular pH-sensitive dye (32,33). Here, we report the direct measurement of extravesicular pH changes associated with the permeability of M2 in vesicles. We used the pH electrode method reported earlier (34,35) to examine the effects of amantadine and variation in pH on M2 function. The protein channel activity was monitored by measuring the change in pH of the weakly buffered external solutions. As with previous studies, determining the number of functional M2 proteins in our assay was difficult because of the possibility of variable incorporation, variable oligomerization (or nonfunctional incorporation), and nonuniform partitioning of the protein into the liposomal membranes. In this study, we have determined the average proton flux/vesicle. Dividing by the nominal number of M2 tetramers/vesicle we determine the time-averaged single-channel conductance of M2. Some of the results have been presented previously in preliminary form (36–38).

MATERIALS AND METHODS

Purification and reconstitution of M2 from *Escherichia coli*

M2 protein was expressed and purified from inclusion bodies using previously published methods (39). Briefly, the M2 protein, Udorn variety with a six-His tag at the C-terminus and serine substitutions for C19 and C50 was expressed in BL21 (DE3) cells using the PET 39 plasmid and purified from inclusion bodies with a Ni affinity column or using diethylaminoethanol. Gel electrophoresis revealed the presence of a single band in a sodium dodecylsulphate gel (Fig. 1). Sequence variants containing a His-tag at the N-terminal, His-tag cleaved with Tobacco Etch Virus (TEV) protease, or His-37 mutated to alanine (H37A) were also expressed and purified similarly and used for the study. Protein concentration was determined using the bicinchoninic acid method. The protein was reconstituted into 1,2-dimyristoyl-*sn*-glycero-3-phosphocholine (DMPC) and 1,2-dimyristotl-*sn*-glycero-3-[phosphoro-rac-(1-glyercerol)] (DMPG) lipids (4:1 molar ratio; Avanti Polar Lipids, Alabaster, AL) at a 1:5 protein/lipid (w/w) ratio using 1% *n*-octyl β-D-glucopyranoside and then dialyzed three times. The dialyzed sample was centrifuged and resuspended as proteoliposomes in aqueous solution.

Reconstitution of M2 protein in liposomes

This step involved two procedures. First, protein-free lipid vesicles were prepared and then mixed with M2 proteoliposomes by freeze-thaw sonication. The size of the resulting liposomes was measured by dynamic light scattering (90Plus particle size analyzer, Brookhaven Instruments, Holtsville,

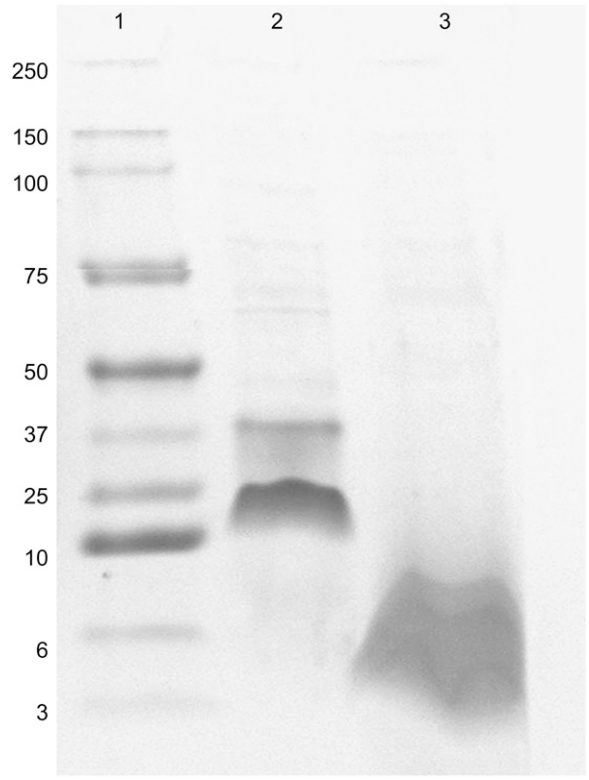

FIGURE 1 SDS-PAGE of reconstituted M2. (*Lane 1*) Apparent molecular weight of a standard ladder. (*Lane 2*) M2 reconstituted in vesicles (DMPC/DMPG 4:1) is free of contaminants. (*Lane 3*) Application of trypsin to proteoliposomes cleaves M2.

NY). For experiments at pH 7.0 and pH 5.4, different intravesicular and extravesicular buffers were used, as described below.

Preparation of lipid vesicles

Stock solutions of L-6-phosphatidlyethanolamine, L-α-phosphatidylcholine, L-6-phosphatidylserine from brain, and cholesterol each at 10 mg/ml in chloroform were mixed to a molar ratio of 4:1:1:2 in a small test tube (hereafter 4112) and evaporated under nitrogen. For pH 7.0, the dry lipids were solubilized in a solution of 120 mM KH_2PO_4, 120 mM K_2HPO_4, 150 mM NaCl, and 20 mM KCl. The solution was titrated to pH 7.0 with KOH. The molarity of total potassium is ~215 mM after mixing 1:1 with M2 vesicles prepared in pure water. This corresponds to a potassium activity inside the fused vesicles of 140 mM. It is lower than total [K^+] because of binding to phosphate. For pH 5.4, the same molar ratio of lipids was used. The dry lipids were solubilized in a solution of 120 mM K_3Citrate, 120 mM KH_2Citrate, and 120 mM NaCl titrated to pH 5.4 with KOH. The molarity of total potassium is ~300 mM after dilution. This correlates with a potassium activity of ~200 mM. Since the vesicles were always diluted 1:100 in translocation buffer (defined below) during the assay, the voltages across the vesicular membrane were about the same at pH 7.0 and 5.4. The suspension was mixed by vortexing vigorously for 10 min. It was then sonicated in a bath sonicator (Sonicor SC-4U, Sonicor Instrument, Copiague, NY) for 4.5 min.

Preparation of M2 mixed-lipid vesicles

Equal volumes of 4112 vesicles and the M2 proteoliposomes were mixed (M2 mixed vesicles) at room temperature, vortexed briefly, and sonicated for 30 s. The combined solution was then frozen to −20°C, thawed at room temperature, and sonicated for 30 s. The freeze-thaw sonication process was then repeated for a total of three cycles. The protein/lipid ratio was 1:10 in the new mixed vesicles with an internal buffer concentration reduced to 50% of the original concentration. Before experimental use, the vesicles were sonicated and the vesicle diameter measured by dynamic light scattering.

Proton flux assay

Proton flux across the vesicle membrane was measured according to the method described by Cao et al. (34) and Franklin et al (35). The translocation buffer for experiments at pH 7.0 was composed of 190 mM Na_2SO_4, 0.1 mM KH_2PO_4, and 0.1 mM K_2HPO_4; for experiments at pH 5.4, it was composed of 190 mM Na_2SO_4, 0.1 mM K_3Citrate, and 0.1 mM KH_2Citrate.

Three milliliters of the translocation buffer were placed in the experimental cuvette and stirred to equilibrate the buffer at room temperature. A highly selective pH probe (AccupHast combination electrode model 13-620-297, Fisher Scientific, Hampton, NH) was inserted. A solution containing 30 μL of M2 mixed vesicles was next added to the cuvette and allowed to equilibrate for ~5 min at room temperature (~23°C), and changes in pH over time were recorded. After the baseline was stable for 2–3 min, 3 μL of the K^+ ionophore valinomycin (25 μg/ml ethyl alcohol, Sigma, Saint Louis, MO) were added to the solution (Fig. 2). After 3–5 min, 7.5 μL of the protonophore carbonyl cyanide m-chlorophenylhydrazone (CCCP, 200 μM in ethyl alcohol, Sigma), were added for calibration. Finally, the solution was back-titrated after 3–5 min with 30 μL of 1 mM HCL. For the duration of the process, the solution was constantly stirred and continuous pH readings were recorded. The concentration of valinomycin is not rate-limiting, as changing its concentration did not significantly change the results. Inhibitor studies were performed in the presence of amantadine by adding 30 μL of 100 mM amantadine to a final concentration of 1 mM and then incubating the M2 mixed vesicles for 5 min before triggering proton translocation. The same procedure was followed to detect the change in the proton flux, namely, addition of valinomycin followed by CCCP, and the standard back-titration.

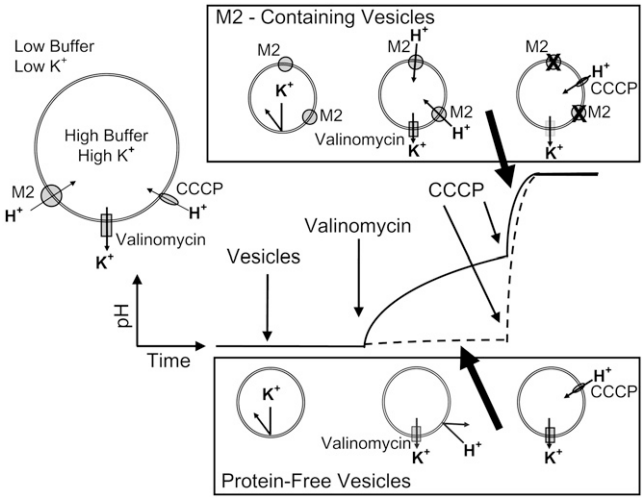

FIGURE 2 Proton flux assay. Proton flux is driven by a membrane potential created when valinomycin is added to vesicles prepared with asymmetric [K^+]. Valinomycin, a potassium ionophore, allows potassium efflux, creating the potential that drives proton influx through M2 protein. Proton-leaky vesicles without M2 also will exhibit flux at this step. CCCP, a protonophore, permits proton influx into vesicles that did not previously discharge their gradient. The pH stabilizes after addition of valinomycin when vesicles reach the Donnan equilibrium for hydrogen and potassium. Activity of K^+ was determined as described in Materials and Methods.

To ensure the stability and integrity of the liposomes, control experiments were conducted in which valinomycin was added at 5, 15, or 45 min after the liposome addition. Control liposomes were prepared in parallel without M2. Average vesicle diameter ranged from 173–218 nm, independent of protein content. Each M2 proton flux was compared to a protein-free experiment under similar conditions.

The analog output of the pH meter was filtered at 20 Hz and amplified 200 times (LPF-8, Warner Instrument, Hamden, CT). The data were collected and stored at 100 samples/s using Labview software (version 7.0, National Instruments, Austin, TX). The data were then averaged at 4 Hz using Excel. All tracings are scaled to the back-titration of 30 nmol HCl performed after each experiment. Drift was subtracted out of each tracing to make clearer the change in slope after valinomycin addition.

Calculation of single-channel proton flux

The time-average proton current of a single channel was calculated from the initial rate of hydrogen influx, converted to current, and normalized to reflect both the extravesicular buffer strength using the back-titration and the predicted number of functional M2 tetramers assuming full incorporation and tetramerization:

$$i = F \cdot J_{0,\mathrm{norm}}/N_{\mathrm{tetramers}}. \quad (1)$$

The initial rate of hydrogen influx was measured experimentally from the initial slope of the pH curve after valinomycin addition and was taken as an average of the steepest and the shallowest lines that could reasonably approximate the slope, which was then converted to hydrogen influx (mol/s), $J_{0,\mathrm{norm}}$, based on the standard back-titration. A typical trace is shown in Fig. 3. Based on the total lipid and protein mass, the average surface area of a lipid molecule, and the surface area of a lipid vesicle, the nominal number of M2 channels/vesicle can be estimated (Table 1). Vesicles that contain no or only inactive M2 make up the CCCP signal and do not contribute to the initial valinomycin pH rise. The flux can be converted to conductance if the hydrogen driving potential is known. The solution inside the vesicles

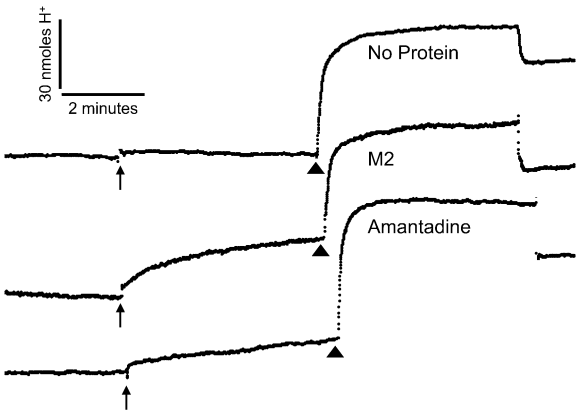

FIGURE 3 M2 proton flux at pH 7.0, as represented by tracings of bath pH (*Upper curve*) Protein-free vesicles show no change in slope after addition of valinomycin, confirming that these vesicles do not leak protons. Addition of valinomycin is indicated by the arrows and addition of CCCP by the arrowheads. The presence of a CCCP signal shows the influx of protons into control vesicles. (*Middle curve*) Vesicles containing M2 show increased proton influx after addition of valinomycin. (*Lower curve*) The proton influx was reduced by preincubating M2 vesicles with amantadine.

contains 150 mM K^+ and the outside contains ~0.2 mM K^+ after the addition of 30 μL vesicle solution to 3 mL translocation buffer. After the addition of valinomycin, the vesicle membrane is estimated to be initially clamped at a potential V_m of ~ -112 mV. The time-averaged single-channel conductance and the single-channel permeability were calculated for the initial symmetrical proton concentration conditions from

$$\gamma = i/V_m \tag{2}$$

and

$$P = \frac{(RT)^2}{(Fz)^3}\gamma. \tag{3}$$

The standard deviations are reported for all measurements in Table 1. These experimental standard deviations are propagated, in the form of variances, to calculations of current and permeability using the following equation:

$$\mathrm{var}\,F(x,y) = \left(\frac{\partial F(x,y)}{\partial x}\right)^2 \mathrm{var}(x) + \left(\frac{\partial F(x,y)}{\partial y}\right)^2 \mathrm{var}(y). \tag{4}$$

There were five protein-free controls at pH 5.4 and four at pH 7.0. There were three M2 experiments at each pH. There were two amantadine experiments at pH 5.4 and three at pH 7.0.

Numerical simulation of proton uptake

Changes in external pH, internal pH, and membrane potential were simulated by numerical integration using the approach given in the Appendix. This traditional compartmental analysis represented the systems as two compartments, interior and exterior, separated by a membrane permeable to H^+ and K^+. The membrane potential is established from the equivalent circuit equation with selective permeability represented as selective conductance. Buffers were assumed to be in instantaneous equilibrium throughout both compartments and membrane permeability was assumed to be low enough relative to bulk diffusion to prevent concentration gradients in compartmental bulk solutions. Unless specified otherwise, the parameters used in the simulations were (aggregate) $G_H = 0.000146$ S ($t = 0$–5 min) and $G_H = 0.00146$ S ($t = 5$–10 min) (see Fig. 7, *a–c* only), $G_K = 0.00146$ S ($t = 0$–10 min), $[K^+]_i = 140$ mM, $[K^+]_o = 1.285$ mM, $pH_i = pH_o = 6.8$, buffer pK = 7.0, $[Buffer]_i = 120$ mM, $[Buffer]_o = 1.188$ mM, and trapped volume = 2.2 μl.

RESULTS

M2 induced pH change

Our objective was to determine the proton permeation and amantadine sensitivity of the M2 protein at pH 7 and pH 5 in lipid vesicles. Previous researchers have induced proton flux into vesicles via an electrochemical gradient (32,35). The proton flux at such low concentrations of hydrogen is very minute. Using an assay similar to Franklin et al. (35), we directly measured the basification of a weakly buffered external solution when proton flux through M2 (reconstituted

TABLE 1 Calculation of single channel current, conductance, and permeability

	Control		M2		M2 + amantadine	
External pH	5.4	7.0	5.4	7.0	5.4	7.0
Potential (mV)	−112	−112	−112	−112	−112	−112
Vesicle diameter (nm)	186 ± 28	196 ± 15	218 ± 32	174 ± 42	218 ± 32	174 ± 42
Total lipid surface area (cm^2)*	760	760	760	760	760	760
Total vesicles ($\times 10^{-11}$)	7.0 ± 0.95	6.3 ± 0.49	5.1 ± 1.5	8.0 ± 2.2	5.1 ± 1.1	8.0 ± 2.2
Total vesicular trapped volume (μL)	2.4 ± 1.1	2.5 ± 0.61	2.8 ± 1.5	2.2 ± 1.7	2.8 ± 1.4	2.2 ± 1.7
Total protein (μg)	0	0	40.5	15	40.5	15
Total number of tetramers ($\times 10^{-14}$)			5.4	2.0	5.4	2.0
Tetramers/vesicle			1050	250	1050	250
Initial slope (mV/min)	4.0 ± 1.6	7.1 ± 2.8	27.6 ± 1.8	31.5 ± 14.3	32.4 ± 21.9	15.6 ± 0.6
Height of 30 nmol H^+ back-titration (mV)	97 ± 36	128 ± 57	75 ± 36	92 ± 30	106 ± 2.0	91 ± 33
H^+/vesicle/s	21 ± 12	32 ± 22	257 ± 122	124 ± 63	226 ± 197	64 ± 23
H^+/tetramer/s			0.24 ± 0.14	0.50 ± 0.29	0.21 ± 0.19	0.26 ± 0.12
Unitary current ($A \times 10^{21}$)			39.1 ± 21.9	80.5 ± 46.9	34.4 ± 30.9	41.3 ± 19.0
Unitary conductance ($S \times 10^{18}$)			0.35 ± 0.20	0.72 ± 0.42	0.31 ± 0.28	0.37 ± 0.17
Proton permeability ($cm^3/s \times 10^{17}$)			2.3 ± 1.3	191 ± 111	2.0 ± 1.8	9.8 ± 4.5

*Assuming 63 $Å^2$/headgroup/leaflet × 2 leaflets/bilayer.

in lipid vesicles loaded with potassium) was induced by the addition of the potassium ionophore valinomycin.

Fig. 2 shows the mechanism of proton transport across vesicles. Potassium efflux creates an initial potential of −112 mV inside the vesicles. This potential drives proton influx into vesicles with functional M2. The proton influx is recorded by measuring the increase in pH of the solution outside the vesicles. Proton influx was not detected in protein-free control vesicles. We did observe a small pH drift in some experiments, presumably due to buffer pK shifts or CO_2 solubility related to thermal equilibration, which has been subtracted from all tracings presented for clarity. Addition of the protonophore, CCCP, serves as a positive control for the presence of vesicles without active protein.

There is a clear increase in M2-mediated proton uptake as measured directly under neutral pH conditions using this method. Fig. 3 shows a typical pH 7 result of pH change owing to proton translocation by M2, as currently constituted. The fast rise in pH immediately after valinomycin addition in the vesicles containing M2 is due to proton movement in response to valinomycin-induced K^+ efflux. This fast signal is not observed in control vesicles. The 10-s slope after initial addition of valinomycin is proportional to H^+ influx. This figure also shows the pH rise after CCCP addition with both M2 and control vesicles. This is due to the exchange of K^+ for H^+ in all vesicles that do not contain active M2. The total signal, a combination of the valinomycin and CCCP signal, is proportional to the total volume entrapped inside the vesicles. Fig. 3 also shows the effect of external amantadine on M2-induced proton flux. Consistent with amantadine block, the valinomycin signal is reduced, indicating the reduction of M2-induced proton flux. Control vesicles treated with 1 mM external amantadine showed no amantadine-induced leak at pH 7 (data not shown).

Experiments at low pH also verify the fact that M2 does not conduct significant numbers of Na^+ or K^+ ions. Fig. 4 shows the proton flux measurements at pH 5.4 using a citrate buffer. There is a detectable rise (proton flux) after addition of valinomycin in the M2 samples. The CCCP signal is similar to that seen at pH 7. The results with external amantadine show that the inhibitory strength of amantadine is decreased at low pH, as the difference in proton flux with amantadine and without amantadine is not very high.

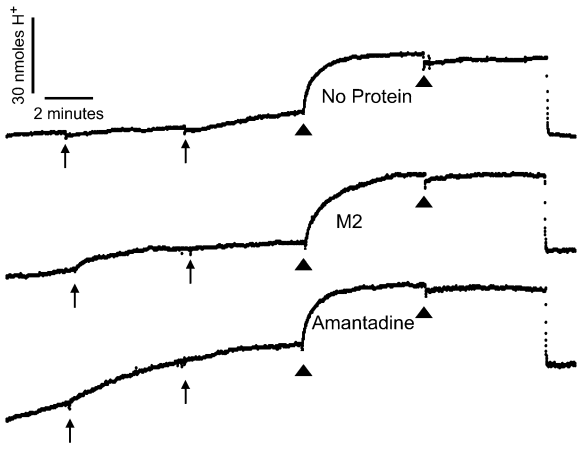

FIGURE 4 M2 proton flux at pH 5.4, as represented by tracings of proton flux into vesicles: (*Upper curve*) Protein-free control vesicles show no change in slope after addition of valinomycin. A second addition of valinomycin seemed to cause a little artifact in control vesicles. (*Middle curve*) M2 increased proton influx after addition of valinomycin. (*Lower curve*) Amantadine block is less effective at pH 5.4. Arrows and arrowheads have the same significance as in Fig. 3.

Analysis of vesicle proton flux

Proton flux through the M2 ion channel was calculated from changes in external pH on the basis of the rate of change in the external free hydrogen $[H^+]$ (calibrated as deduced from the back-titration and the nominal number of tetramers in the experiment (Table 1)). The average sizes of control vesicles, determined by dynamic light scattering, are not significantly different from those of M2-containing vesicles. The buffer capacities were similar for the two pH conditions, with the initial pH 0.2 pH-units below the buffer pK in each case.

Assuming a surface area of 63 $Å^{-2}$/phospholipid headgroup and the average vesicle diameters listed in Table 1, there were 5–8 × 10^{11} vesicles in the experimental samples, corresponding to a trapped volume of 2.2–2.8 μl. The amount of total protein used at pH 5.4 was 40.5 μg, whereas at pH 7.0 the amount used was 15 μg. Assuming that all of the protein was incorporated and in the functional tetramer configuration, there were 1050 channels/average-sized vesicle in the pH 5.4 experiments and 250 in the pH 7.0 experiments. Table 1 shows that changing the pH from 5.4 to 7.0 has no significant effect in number of protons/tetramer/s.

To estimate the single-channel conductance, we divided the difference between the total proton current/vesicle (determined from the back-titration-normalized external pH initial slope and the number of vesicles in the experiment) and that in the control experiment (due to a small amount of proton leakage through the vesicular bilayer) by the nominal number of channels in a single vesicle. At pH 7, the total proton influx into M2-containing vesicles after the addition of valinomycin was 124 ± 63 H^+/vesicle/s. Adjusting for the number of tetramers and the membrane potential, this total influx gives a hydrogen flux of 0.50 ± 0.29 protons/tetramer/s, which corresponds to a time-averaged single-channel conductance of 0.72 ± 0.42 aS. At pH 5.4, these values are 257 ± 122 H^+/vesicle/s, 0.24 ± 0.14 H^+/tetramer/s, and 0.35 ± 0.20 aS. Because the fraction of tetramers that are functional is unknown, these values represent lower limits on single-channel conductance.

A high concentration of amantadine (1 mM) was used to maximally quench M2 activity. Fig. 3 shows that amantadine

reduced the initial proton translocation rate, as quantified in Table 1. We see a 49 ± 38% reduction of M2 proton flux in the presence of amantadine at pH 7 (0.50 vs. 0.25 protons/tetramer/s). At pH 5.4 the amantadine sensitivity is reduced by 12 ± 93% (0.24 vs. 0.21 protons/tetramer/s). Amantadine is known to block exclusively from the N-terminal side (3). Presuming the orientation of the protein to be random in lipid vesicles, we only expect 50% oriented to each side and therefore a 50% block of proton conductance. Although this is the amount of block observed at pH 7, the block is not statistically significant at either pH.

Selectivity of M2

The rise in pH after addition of valinomycin (the valinomycin signal) is inherently dependent on the maintenance of a potassium gradient. If the lipid membrane or M2 channels were to leak potassium it would confound our studies. To examine the leak of potassium through M2, we stirred the vesicles for 5, 15, or 45 min before the addition of valinomycin (Fig. 5). The 5-min prevalinomycin stir time is standard for all experiments, allowing the reaction conditions to stabilize. The 15-min stir shows a CCCP signal that is reduced by 13% when compared to the 5-min stir. Consistent with this observation, the 45-min stir shows a 34%-reduced CCCP signal. Protein-free control vesicles showed that even after 45 min the vesicles were stable, demonstrating that the lipid bilayers were tight enough to maintain the K^+ gradients (data not shown). In contrast, introduction of valinomycin elicited an immediate pH increase. Clearly, valinomycin enabled the K^+ efflux necessary to drive proton flux through M2.

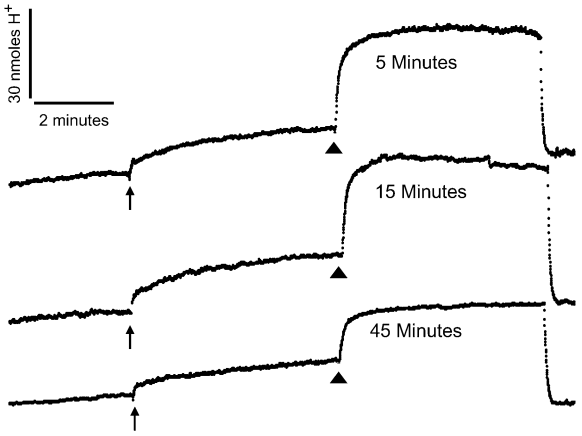

FIGURE 5 Time series. Vesicles were stirred for 5, 15, or 45 min before the addition of valinomycin. (*Upper curve*) Our normal protocol involves a 5-min prevalinomycin stir. (*Middle curve*) A 15-min prevalinomycin stir showed a 13% reduction in total signal compared to the 5-min stir. (*Lower curve*) The 45-min stir showed a 34% reduction in the total signal compared to the 5-min stir. As the control vesicles showed no reduction even after 45 min, the reduction seen in proteoliposomes is attributed to leak of potassium through M2. Arrows and arrowheads have the same significance as in Fig. 3.

As a test of the degree of selectivity implied by the existence of a valinomycin signal, experiments were also performed with gramicidin, a known H^+-, Na^+-, and K^+-permeable channel. At a low gramicidin surface density (0.5 μg/mL), gramicidin exhibited proton flux into vesicles (Fig. 6), presumably because the H^+ permeability is relatively high and the K^+ gradient was retained on the 5-min timescale. At higher densities, gramicidin eliminated the CCCP signal, presumably by leaking potassium from the vesicles. Of additional interest is the fact that, although we used the same method of preparation, namely a 3×-freeze-thaw-sonication fusion of channel-containing and channel-free vesicles, the product shows a homogenous distribution of the channel, demonstrating that vesicle fusion is essentially quantitative. At high concentrations of gramicidin, the CCCP signal is greatly reduced, indicating that few gramicidin-free vesicles persist after the fusion process.

DISCUSSION

M2-facilitated pH change

Vesicle-uptake assays are inherently complicated because of the interactions of multiple driving forces. In the assay used here, we start with no pH gradient and with outward K^+ and inward Na^+ gradients. We then add a K^+ ionophore to initiate K^+ efflux, which in turn leads to a negative membrane potential. The membrane potential drives proton influx into vesicles with M2 present, but not into tight, protein-free vesicles, which exhibit proton influx only after addition of CCCP (a protonophore). Using similar techniques with both

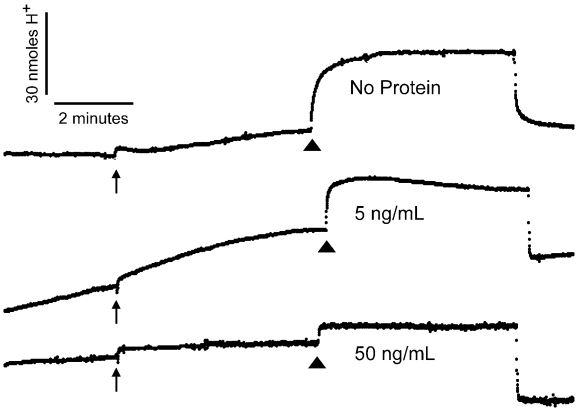

FIGURE 6 Effect of gramicidin on the proton flux assay. Vesicles containing gramicidin were prepared in a manner similar to M2 containing vesicles. The final concentration of gramicidin was 0, 5, 50, or 500 (not shown) ng/mL. (*Upper curve*) Protein-free control shows no valinomycin signal. (*Middle curve*) At 5 ng/mL gramicidin, compared to control, twice the slope was observed after addition of valinomycin. There was also a reduced total signal, suggesting potassium leakage through gramicidin. (*Lower curve*) Gramicidin at a concentration of 50 ng/mL was sufficient to eliminate any response to valinomycin and CCCP. Higher concentrations also showed no signal (data not shown). Arrows and arrowheads have the same significance as in Fig. 3.

valinomycin and monensin for K^+ or Na^+ gradients, respectively, Lin and Schroeder (32) used intravesicular pyridine fluorescence to demonstrate that vesicle pH modification (acidification or basification) proceeds as expected under the assumption that M2 is impermeable to Na^+, K^+, or other bath ions. In this study, we measured the proton influx directly, as a decrease in extravesicular $[H^+]$, using a proton-sensitive electrode.

To help interpret the time course of pH changes, we simulated the flux through an ensemble of vesicles with total trapped volume V, each containing H^+ and K^+ conductance pathways, using numerical integration to solve a system of buffer, equivalent-circuit, and flux equations (see Appendix). The equations describe the relaxation of a system perturbed away from Donnan equilibrium at $t = 0$. Because there are two permeable ions, the system returns quickly to Donnan equilibrium, a state in which the Nernst potential for both ions equals the membrane potential, with a time course that depends on changes in ion content inside and outside the vesicles as a result of ion flux down electrochemical gradients. The equations neglect osmotic effects, which are expected to be small, because ion exchange is essentially obligate.

The slope of the valinomycin signal is insensitive to relative permeability of M2 to K^+ because of the addition of the K^+ ionophore, which is orders of magnitude more permeable. Likewise, the height of the valinomycin signal is sensitive not to the selectivity, but rather to the quantity of bufferable acid inside the vesicles. Nevertheless, the time-series experimental design (used in Fig. 5) does allow quantitation of permeability ratios due to the leakage of K^+ out of vesicles before the addition of valinomycin. Additionally, by inducing vesicle K^+ leakage with gramicidin (Fig. 6), which has known selectivity, we confirm our analysis of the M2 permeability based on the total signal, which is controlled by the remaining buffer strength at the time valinomycin is added. This analysis demonstrates that one cannot determine in a single assay the degree to which protons are more permeable than Na^+ or K^+ ions. It also gives a clearer idea of the time course of the driving forces on the protons. Thus, we next present the results of our simulation in some detail to provide a context for our subsequent interpretations.

Our analysis assumes a set of conditions that are fairly typical and consistent with our experimental conditions, namely, that the solute concentrations were those used in our experiments; the aggregate H^+ conductance was 2×10^{-4} S (similar to that observed in a typical experiment with 2×10^{14} channels conducting 0.50 ± 0.29 protons/tetramer/s for an aggregate proton conductance of 1.46×10^{-4} S); pH = pK − 0.2 inside and outside the vesicles; and at time 0, the K^+ conductance was increased to 2×10^{-3} S by addition of valinomycin, with no other ions permeant. The calculated time courses of the change in free internal and external $[H^+]$ are shown in Fig. 7 *a*. After increasing H^+ conductance at $t = 5$ min to represent CCCP addition, the external pH rises slightly over the course of ~1 min, whereas the internal pH drops nearly 2 pH units over the same time course. We note that, in our experiments, even the high concentration of buffer inside the vesicles is still insufficient to hold the internal pH constant in the face of the large proton influx, even though buffering was assumed to be instantaneous. This is because, even with the high buffer concentrations used here, the K^+ content of the vesicles, which contain only a small fraction of the total volume, exceeds the buffered H^+. Nevertheless, the change in external pH is readily measurable, as was seen experimentally in Fig. 3.

Relaxation to the Donnan equilibrium is attained ~1 min after increasing G_H. This is demonstrated in Fig. 7 *b*, which

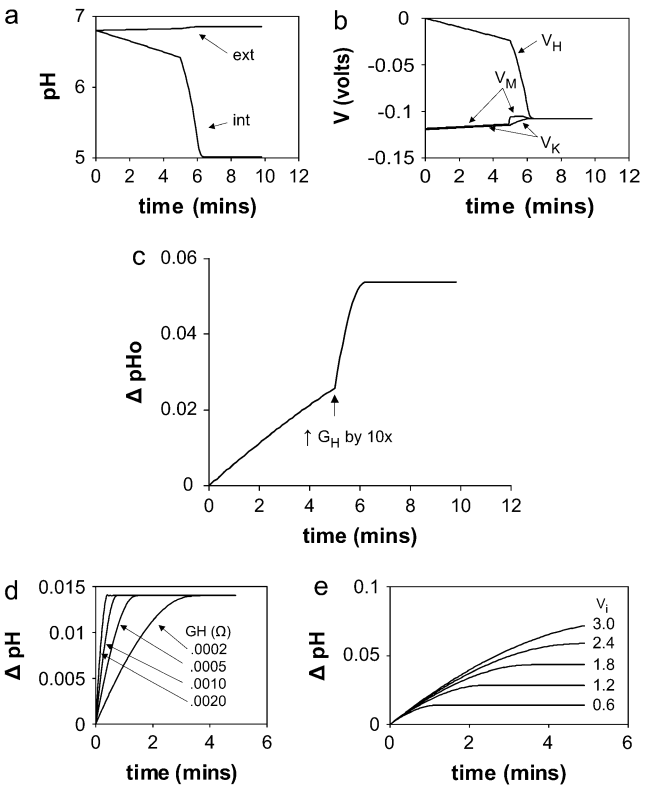

FIGURE 7 Theoretical prediction for the rate of establishment of Donnan equilibrium in a system with two permeable ions. At time zero, G_K is increased, to represent the addition of valinomycin; with $G_K = 0$, baseline is flat before this point. The 10-fold increase in G_H at 5 min is intended to represent the addition of CCCP (*a*) The external (bath) pH rises slightly, whereas the internal (intravesicular) pH falls rapidly, particularly after the increase in G_H at $t = 5$ min. (*b*) Membrane potential and Nernst potentials for H^+ and K^+ from the same simulation as in *a*. (*c*) Expanded view of the external pH trace on a scale similar to that used for experimental traces. Differences in shape between calculated and experimental traces could reflect membrane incorporation times for valinomycin or CCCP, which are assumed to be instantaneous in the simulation. (*d*) Increased G_H results in complete Donnan equilibration in <5 min. The initial slope is proportional to G_H. (*e*) The height of the valinomycin peak depends on the trapped volume, as shown here for volumes given in μl, as well as on internal nonprotonated buffer concentration and internal $[K^+]$ (data not shown). The initial slope is not dependent on these factors, as long as it is determined during the first 20 s after initial ionophore addition. For this simulation, G_H was set to 0.0006 S (with G_K 10-fold higher) to speed equilibration.

shows the time dependence of the Nernst potentials for K^+ (V_K) and H^+ (V_H,), and the membrane potential (V_m) under the same conditions as in Fig. 7 *a*. Acidification of the vesicles is accompanied by a loss of driving force on H^+, as shown by the decline in the Nernst potential for H^+, V_H. The membrane potential, V_m, is sandwiched between V_H and the Nernst potential for K^+, V_K. At $t = 5$ min, V_m abandons its proximity to V_K temporarily because G_H is set to G_K, so V_H contributes more heavily to the equivalent circuit equation for V_m (Eq. A4). V_H, V_K, and V_m merge at the Donnan equilibrium point.

In Fig. 7 *c*, the time course of the external pH is amplified to show that the slow rise obtained, due to the conductance of H^+ from M2 alone, gives way to a rapid rise if H^+ transporters, such as CCCP, are added to the system.

Additional analysis with this simple mathematical model allowed us to determine the following properties of the experimental system:

1. The initial slope of the change of external $[H^+]$ versus time is proportional to G_H, as long as $G_H < 10G_K$ (Fig. 7 *d*). After normalizing for buffer capacity using the average of the back-titration steps, the time-averaged single-channel current times the number of channels, i.e., G_H, is obtained directly from the initial slope, as expected. The initial rate of rise purely reflects G_H to the extent that it is rate-limiting.
2. The rate of rise in pH_o varies when the initial value of $pH - pK_d$ is changed, but this deviation is compensated when one normalizes with the back-titration.
3. The external pH reached a plateau when the membrane potential reached a constant value, corresponding to the establishment of Donnan equilibrium.
4. The height of the pH signal change depended strongly on the vesicular (trapped) volume (Fig. 7 *e*) and the inside and outside buffer concentrations (data not shown), but not discernibly on G_H.
5. Whether the equilibrium membrane potential is nearer to the initial V_H or the initial V_K depends primarily on the relative internal concentrations of buffered H^+ and K^+ (data not shown). Specifically, it is closer to V_H if there is more buffered H^+ inside and closer to V_K if there is more K^+ inside. In the conditions used in our experiments, initial $V_m \approx -112$ mV (Fig. 7 *b*).

One might wonder what happens if the membrane is permeable both to H^+ and K^+ at the outset (i.e., if the M2 channel is imperfectly selective), say for $P_H > P_K$. Although one might expect the driving force on protons to be small, because the membrane potential approaches V_H, the electroneutrality-required obligate exchange still causes proton uptake under an outwardly directed K^+ gradient. If the internal free buffer content is less than the internal K^+ excess (relative to external K^+), a $[H^+]$ gradient will still develop and V_H and V_m will settle near to the original V_K once the Donnan equilibrium is achieved. The kinetics of the relaxation in pH and V_m are governed by the K^+ flux, and hence by the P_K rather than the direct electrochemical driving force on H^+. This argument justifies the conclusions of Lin and Schroeder (2001) concerning high M2 selectivity.

The argument does not apply directly to electrophysiological voltage clamp studies (e.g., Chizhmakov et al. (3)). To the extent that the cytoplasm pH and $[Na^+]$ are well buffered by the patch-clamp pipette, the cell will not relax to a Donnan equilibrium. However, it does raise some questions about the extent and timing of Na^+ contamination of the very small volumes in the cytoplasm and patch pipette, which conceivably may become sufficient to produce an artifactually high apparent selectivity for H^+ over Na^+.

These differences highlight the difficulty in reconstitution assays. Both whole-cell patch-clamp studies (3) and the reconstitution assay used here measure the activity of M2 populations and extrapolate findings to single-channel properties. Precise determination of M2 protein concentration is difficult in either type of study due to contaminating proteins that may be natively expressed in the cell studies or may copurify with M2 in the reconstitution studies. However, reconstitution assays are further complicated by the possibility of protein inactivation during isolation, by random fluctuations of protein insertion into lipid vesicles, and by fluctuations in vesicle diameter. We suspect that the latter factor contributes most to the interexperimental standard deviations in our studies (see also Amantadine block, below).

At the same time, the simulations help explain why gramicidin A, which is known to have a finite permeability to K^+ and Na^+ ($\sim$1/10 that of H^+) can still yield a valinomycin signal on the several-minute timescale of our experiments (Fig. 6). If permeability to H^+ exceeds that to the metal ion, the initial driving force on H^+ is low. However, if the internal K^+ content exceeds the internal buffered H^+, electroneutrality-required exchanges of H^+ for K^+ must be made to drive H^+ into the vesicle until the internal buffer is overwhelmed, and a valinomycin signal is observable.

Quantitative comparison to previous results

Lin and Schroeder (1) reported 7.3 protons/tetramer/s at pH 7.4 and a single-channel conductance of 8×10^{-18} S (at 18°C), $\sim$10 times higher than our results. In our experiments, we took the initial slope from the 10-s interval starting 3 s after the addition of valinomycin. The initial jump (first 3 s) was ignored as an artifact of solvent addition rather than vesicle uptake. Lin and Schroeder do not mention any solvent artifacts, but in the published figures there is a sharp discontinuity in slope during the first second and the second and subsequent seconds. The shape of the approach to equilibrium in our simulations (Fig. 7 *c*) is roughly that of an exponential, so it is clear that the relevant initial slope is that of the segment leading up to the Donnan plateau. Perhaps they focused on an earlier section of the relaxation curve, and thus obtained a slope biased toward a higher value. This could explain why we estimate the time-averaged single-channel

conductance and permeability to be lower, 7.2×10^{-19} S at pH 7.0 at 22°C. Alternatively, our protein may be less active (incorporated or well-configured) than theirs. It is not possible from the data presented here to distinguish between these possibilities.

If one could make assumptions about the impact of pH on single-channel conductance (via mass action) and acid-gating, it would now be possible to relate this to the measured single-channel conductance of the open state, ~6 pS for this same preparation at pH 3 in planar bilayers (8). For instance, we could assume that the conductance of the open state is proportional to $[H^+]$ (with no saturation) and ignore any acid-gating effects to extrapolate an open-state conductance at pH 6.8 of 0.95 fS. By comparison to the measured time-averaged conductance of 0.72 aS, we would deduce that $P_o = 7.7 \times 10^{-4}$, one order of magnitude larger than that observed in the planar bilayers (assuming that each bilayer experiment resulted from the fusion of one vesicle containing the nominal number of fully active tetramers), i.e., 7.5×10^{-5} (8). However, the acid-gating phenomenon has been well established in electrophysiological experiments (3), saturation is known to occur below pH 8.5 (3,8), and the vesicle uptake results do not confirm the expectation of mass action, which point we discuss next.

Acid activation

Based on cell acidification (2), electrophysiological (3,31), and vesicle acidification (32) experiments, it is frequently stated that M2 is acid-gated. Solid-state NMR measurements of the titration states of a peptide consisting of the transmembrane domain from M2 (40) indicate that two of the four His residues in the selectivity filter are protonated, with a pKa of 8.2, the third is protonated at pH 6.3, and the fourth is protonated at pH < 5. This indicates that it is the third His-37 protonation that correlates with acid gating in electrophysiological (3,5) and fluorescence studies (11,41). Care has to be exercised in the interpretation of the effects of acidification on hydrogen conductance to distinguish the effects of mass action (passive electrodiffusion) from effects attributable to changes in protein conformation or dynamics. Nevertheless, a secure claim for acid gating can be found in the result that basification of the extracellular fluid decreases outward H^+ current through M2 channels despite an increased outward electrochemical driving force (2,3). The effect seems to be greatest when the N-terminus of M2 is exposed to the more basic solution, although some effect is seen in both directions (4).

In this regard, we were somewhat surprised that our measured H^+ single-channel permeabilities were not increased dramatically at lower pH. Lin and Schroeder (32) observed a twofold increase in flux at pH 5.7 (compared to pH 7.4) and we observed a slight decrease at pH 5.4 (compared to pH 7.0). However, we expect H^+ influx to be increased at the lower pH in both cases by a factor of 40–50 due to mass action, and by some additional factor because of acid gating. This lack of mass action and acid activation occurs in both studies, although they differ in protein species (Weybridge versus Udorn), lipid membrane compositions, and palmitoylation and phosphorylation states of the protein (Lin and Schroeder used the *Trichoplusia ni* insect cell expression, whereas we used the *E. coli* bacterial expression system). Changes in pH over approximately the same range lead to an ~10-fold increase in proton conductance in electrophysiological studies with cell expression systems (3). Taken at face value, one could conclude that lipid-protein interactions cause different behavior in purified reconstituted systems and cell expression systems.

The observation that proton channels and transporters could have a constant H^+ flux over a large range of H^+ bulk concentrations has been noted in other systems. Many studies with proton transporters (35,42) suggest that proton transport is pH-independent in physiological conditions. For instance, Feniouk et al. (43) recently measured proton conductance for F_O in chloroplasts, finding it to have a weak dependence on pH and a higher unitary conductance than expected from gramicidin measurements. They attributed these behaviors to proton buffering by protein side chains along the transport pathway. In this case, residues near or in the selectivity filter may have a buffering role. Similar behavior is shown at near-neutral pH by proteins that form channels, as summarized in DeCoursey (42). One might consider that the pH near the mouth of the channel is buffered by the lipid headgroup region, or that the kinetics of proton approach to the channel are modulated by bulk buffer (44). We suppose, in our experiments, that an obligatory site in the transport pathway is saturated at pH 7.0 whose H^+ dissociation rate constant is approximately the same at pH 5.4 as at pH 7.0. It is possible that acid activation may occur above pH 7.0 or below pH 5.4.

M2 variants

In addition to those data shown, we conducted preliminary proton-flux studies with various mutants of M2, including one with the His_6 tag used for purification in either the N-terminal or C-terminal positions, one without the His_6 tag (TEV-cleaved), and one with fluorination of Trp-41. All show similar signals, indicating that these mutated samples also primarily conduct protons and that the proton flux is not affected by these mutations. Proton flux studies with reconstituted Udorn M2 provided by Dr. Larry Pinto's group and reconstituted Weybridge M2 provided by Dr. Alan Hay's group have also been studied in our lab with similar flux results. From these results, it appears that quality of the incorporation and the level of functionality are similar for all three preparations.

Amantadine block

Preincubation of the sample with 1 mM extravesicular amantadine resulted in a lower initial slope after addition of valinomycin, which corresponds to a final flux of 0.26 ± 0.12

protons/tetramer/s at pH 7.0 and 0.21 ± 0.19 protons/tetramer/s at pH 5.4. These equate to a single-channel conductance of 0.37 ± 0.17 aS and 0.31 ± 0.28 aS, respectively. Thus, M2 is inhibited 49 ± 38% at pH 7.0 and 12 ± 93% at pH 5.4. Although the M2 affinity for amantadine is known to be 10 μM (31), we chose to use 1 mM to obtain maximal block. At such high concentrations of amantadine, we expected 100% block of M2 for those channels with the N-terminus of the monomers projecting out of the vesicles (3). Lin and Schroeder established that M2 in their preparations was randomly oriented such that half of the N-termini were inside and half were outside. Assuming that the M2 tetramers in our proteoliposomes are also randomly oriented, we expect proton flow to be inhibited by 50%, as we observed at pH 7.0. The degree of block was reduced at pH 5.4, as expected from electrophysiological experiments where K_i increases ~50% upon change in pH from 7.5 to 6.2 for Udorn M2 (31), and possibly much more at pH 5.4. In addition, low pH might enhance protein orientation in the membrane such that the amine terminus is inside the vesicles, rendering them resistant to amantadine.

However, having reviewed these issues, it is more important to note that quantitative fluctuations in valinomycin-induced uptake from experiment to experiment make it difficult to achieve statistical significance. To contrast initial slope without amantadine to initial slope with amantadine, separate experiments are required, meaning separate vesicle populations. Statistical significance may require obtaining more uniform vesicle populations, which might be achievable using multiply extruded vesicles (which could, however, affect protein concentrations) and/or more samples than were used here.

Selectivity of M2

Lin and Schroeder estimated, based on the lack of baseline drift and contrary ionophore signal, that M2 was essentially perfectly selective for protons in the presence of high concentrations of potassium. We evaluated this conclusion in our system by stirring the proteoliposomes for 5, 15, or 45 min before addition of valinomycin (Fig. 5). The 15-min stir showed a 13% reduction in total signal compared to the 5-min stir and provides evidence that, on the relevant timescale (10 min), the vesicles remain relatively selective against potassium.

A 34% reduction in total signal after stirring for 45 min compared to 5 min was also observed at pH 7. Protein-free liposomes did not show reduced signal even after a 45-min prevalinomycin stir (data not shown). This suggests that, in addition to protons, M2 also transports other ions, including potassium. Assuming that all vesicles in the experiment represented in Fig. 5 lost 34% of their membrane potential driving force due to a reduction in V_K, over 40 min, we estimate that the K^+ influx over the 40-min period was 0.25 ions/tetramer/s. This K^+ flux is equivalent to a permeability of 8×10^{-23} cm^3/s. Comparing permeabilities, M2 is selective for H^+ over K^+ by a factor of $\sim 10^7$.

To further examine the dependence of our assay on the selectivity of M2, experiments were also performed with gramicidin A (Fig. 6), which is selective for H^+ over K^+ by a factor of ~10 (45). In our experiments, when gramicidin was reconstituted into liposomes at concentration of 50–500 ng/mL, the entire potassium gradient (membrane potential) was lost after only 5 min incubation and stirring in the low-K^+ buffer. At the lower dose of gramicidin (5 ng/mL) the proton influx is similar to that observed with M2, indicating that even with a moderate amount of nonselective leakage, preservation of a significant portion of the potassium gradient over 10 min is possible.

Incorporation, tetramerization, and open-state probability

We do not yet have a good measure of incorporation and tetramerization for M2 reconstituted into vesicles, but preliminary evidence from NMR studies indicates that protein incorporation is variable and incomplete under the conditions used to date. However, to provide upper limits, we continue the assumption of complete incorporation used previously, extending it as well to gramicidin A incorporation; and we examine how the slope in the M2 signal compares to that of the gramicidin A signal.

At 5 ng gramicidin A/mL there are ~6 gramicidin monomers/vesicle or 8×10^{-11} mol/cm^2. Assuming the dimerization constant determined with dansylated gramicidin fluorescence studies ($K = 2 \times 10^{13}$ cm^2/mol in painted dioleoylphosphatidylcholine bilayers (46)), at this concentration the equilibrium is heavily biased (99%) toward dimers, yielding 3 dimers/vesicle. For M2, the tetramer → dimer dissociation constant for M2 was measured with analytical centrifugation to be 4×10^{-21} M (47). To determine the fraction of tetramers in our experiments, based on the Kochendoerfer et al. model, we compared our lipid concentration and M2 monomer concentration to their concentrations of detergent and M2 protein. According to their model analysis, the tetramer would comprise a protein weight fraction of ~0.9, with a fraction of ~0.1 containing monomers and octamers at our protein density. Hence, for a typical vesicle at pH 6.8, 90% of the mass or 222 tetramers/vesicle would be in the tetramer state. Qualitatively, it appears that the initial H^+ flux with 5 ng/ml gramicidin A, corresponding to 3 channels/vesicle (Fig. 6) is similar to that with M2, suggesting that gramicidin A is 74 times more active than M2. The single-channel conductances for the two channels are similar at lower pH (8), so we attribute the higher activity of gramicidin to a higher probability that the dimer channel is open, i.e., in the conducting state. On this basis, for the conditions of peptide density used here, the P_O for the gramicidin dimer is 1.0, and we estimate the P_O for the M2 tetramer to be 0.014, similar to values estimated from single-channel conductance studies (8).

In summary, the proton-flux assay has the potential to provide accurate in vitro measurements of the activity of M2

channel populations. If protein concentration and activity are known, this can be extrapolated to average single-channel properties. This work reports our first attempts to measure proton flux through the M2 protein reconstituted into lipid vesicles. We conclude that the proton-flux assay, whether measuring by internal pH-sensitive dye or external-bath pH-sensitive electrode, provides a valid quantitative measurement of time-averaged channel population conductance, as supported by our modeling. We also conclude that M2 reconstituted from inclusion bodies is amantadine-sensitive and is selective for H^+ over K^+ by several orders of magnitude, as supported by the gramicidin and the time series experiments. Based on the single-channel conductances obtained with the same preparation and the nominal channel density in the vesicle membrane, the single-channel open-state probability is between 10^{-6} and 10^{-4}. Assuming the same open-state probability, the unitary conductance at pH 5.4 is not significantly different from that at pH 7.0. Lin and Schroeder's significant result of a twofold increase defies the large increase (50×) in conductance predicted by mass action and we conclude that there is no evidence for acid gating in either study. There are many parameters yet to be studied, such as dose-response curves for M2 and amantadine, internalization of amantadine, reconstituting M2 by various methods such as dialysis, more thoroughly measuring proton flux with changes in pH for studying acid activation and His-37 titration, and evaluation of M2 protein orientation in smaller vesicles. Future research will lead to finer control of these variables.

APPENDIX

We assumed that buffer equilibration was instantaneous on the timescale of membrane flux. The analytical solution to the differential equation was assumed to be too difficult to obtain due to the contributions of driving forces for two ions, one buffered according to

$$HP \leftrightarrow H^+ + P^-$$
$$K_d = \frac{[H^+][P^-]}{[HP]} \tag{A1}$$

The algorithm used was as follows.

1. From the initial pH inside and outside of the vesicles, the initial total [H] = [H^+] + [HP] (i.e. free hydrogen plus hydrogen buffered by phosphate) is first calculated from the free H^+, [H^+], and the total buffer (phosphate) concentrations, [P], on each side. For this, Eq. A1 is converted to a quadratic equation in [H^+] with only [P] and [H] as parameters by substituting [H^+] − [H] + [P] for [P^-] (the unprotonated buffer) and [H] − [H^+] for [HP], both based on conservation of matter, into Eq. A1 to obtain

$$[H^+]^2 + ([P] - [H] + K_d)[H^+] - K_d[H] = 0 \tag{A2}$$

Solving A2 for [H],

$$[H] = \frac{K_d + [H^+] + [P]}{1 + \frac{K_d}{[H^+]}} \tag{A3}$$

Because the first two terms of the numerator are negligible, the bound and free proton concentrations comprise ~½ the total buffer concentration when pH = pK, as expected. This equation allows us to explore conditions where pH ≠ pK.

2. The initial membrane potential is computed for selected conductance parameters using the equivalent-circuit equation, with the assumption that only H^+ and K^+ are permeant, and computing the Nernst potentials, V_H and V_K, from the initial concentrations inside and outside the vesicles:

$$V_m = \frac{G_H V_H + G_K V_K}{G_H + G_K}. \tag{A4}$$

3. The flux for each species, in mol/s, is taken from the ionic current using the same conductance and driving-force parameters:

$$J = \frac{G_S}{F}(V_m - V_S), \tag{A5}$$

where $S = H^+$ or K^+.

4. The change in total concentration for each ion on each side in a short time, Δt, is taken as

$$\Delta[S] = \frac{J\Delta t}{V}, \tag{A6}$$

where $S = H^+$ or K+, the sign of the change depends on the direction of flux, and V is the volume of the compartment being calculated, intra- or extravesicular. The time step must be small enough to allow only an incremental change in ion concentrations on each side.

5. Finally, the new free H^+ concentration is computed in each compartment, assuming instantaneous buffer equilibration, from the new [H]s inside and outside using the rational solution of Eq. A2, namely

$$[H^+] = (-A + (A^2 + 4K_d[H])^{1/2})/2, \tag{A7}$$

where $A = [P] - [H] + K_d$.

This algorithm was then iterated repeatedly until a steady state was achieved. The initial point was taken as the time of addition of valinomycin to create $G_K > 0$, assuming a preexisting $G_H > 0$ via M2 channels.

We acknowledge the help of Matthew A. D'Haenens, Brad L. Rogers, Lane D. Squires, and Steven D. Later with experiments and simulations.

This work was funded by National Institutes of Health grants AI23007 and GM61272.

REFERENCES

1. Hay, A. J. 1992. The action of adamantanamines against influenza A viruses: inhibition of the M2 ion channel protein. *Semin. Virol.* 3:21–30.
2. Pinto, L. H., L. J. Holsinger, and R. A. Lamb. 1992. Influenza-virus M2 protein has ion channel activity. *Cell.* 69:517–528.
3. Chizhmakov, I. V., F. M. Geraghty, D. C. Ogden, A. Hayhurst, M. Antoniou, and A. J. Hay. 1996. Selective proton permeability and pH regulation of the influenza virus M2 channel expressed in mouse erythroleukaemia cells. *J. Physiol.* 494:329–336.
4. Chizhmakov, I. V., D. C. Ogden, F. M. Geraghty, A. Hayhurst, A. Skinner, T. Betakova, and A. J. Hay. 2003. Differences in conductance of M2 proton channels of two influenza viruses at low and high pH. *J. Physiol.* 546:427–438.
5. Mould, J. A., J. E. Drury, S. M. Frings, U. B. Kaupp, A. Pekosz, R. A. Lamb, and L. H. Pinto. 2000. Permeation and activation of the M-2 ion channel of influenza A virus. *J. Biol. Chem.* 275:31038–31050.
6. Mould, J. A., H. C. Li, C. S. Dudlak, J. D. Lear, A. Pekosz, R. A. Lamb, and L. H. Pinto. 2000. Mechanism for proton conduction of the M-2 ion channel of influenza A virus. *J. Biol. Chem.* 275:8592–8599.

7. Venkataraman, P., R. A. Lamb, and L. H. Pinto. 2005. Chemical rescue of histidine selectivity filter mutants of the M2 ion channel of influenza A virus. *J. Biol. Chem.* 280:21463–21472.
8. Vijayvergiya, V., R. Wilson, A. Chorak, P. F. Gao, T. A. Cross, and D. D. Busath. 2004. Proton conductance of influenza virus M2 protein in planar lipid bilayers. *Biophys. J.* 87:1697–1704.
9. Howard, K. P., J. D. Lear, and W. F. DeGrado. 2002. Sequence determinants of the energetics of folding of a transmembrane four-helix-bundle protein. *Proc. Natl. Acad. Sci. USA.* 99:8568–8572.
10. Salom, D., B. R. Hill, J. D. Lear, and W. F. DeGrado. 2000. pH-dependent tetramerization and amantadine binding of the transmembrane helix of M2 from the influenza A virus. *Biochemistry.* 39:14160–14170.
11. Okada, A., T. Miura, and H. Takeuchi. 2001. Protonation of histidine and histidine-tryptophan interaction in the activation of the M2 ion channel from influenza A virus. *Biochemistry.* 40:6053–6060.
12. Wang, J. F., S. Kim, F. Kovacs, and T. A. Cross. 2001. Structure of the transmembrane region of the M2 protein H^+ channel. *Protein Sci.* 10: 2241–2250.
13. Kovacs, F. A., and T. A. Cross. 1997. Transmembrane four-helix bundle of influenza A M2 protein channel: structural implications from helix tilt and orientation. *Biophys. J.* 73:2511–2517.
14. Pinto, L. H., G. R. Dieckmann, C. S. Gandhi, C. G. Papworth, J. Braman, M. A. Shaughnessy, J. D. Lear, R. A. Lamb, and W. F. DeGrado. 1997. A functionally defined model for the M-2 proton channel of influenza A virus suggests a mechanism for its ion selectivity. *Proc. Natl. Acad. Sci. USA.* 94:11301–11306.
15. Nishimura, K., S. G. Kim, L. Zhang, and T. A. Cross. 2002. The closed state of a H^+ channel helical bundle combining precise orientational and distance restraints from solid state NMR-1. *Biochemistry.* 41:13170–13177.
16. Duong-Ly, K. C., V. Nanda, W. F. Degrado, and K. P. Howard. 2005. The conformation of the pore region of the M2 proton channel depends on lipid bilayer environment. *Protein Sci.* 14:856–861.
17. Kovacs, F. A., J. K. Denny, Z. Song, J. R. Quine, and T. A. Cross. 2000. Helix tilt of the M2 transmembrane peptide from influenza A virus: an intrinsic property. *J. Mol. Biol.* 295:117–125.
18. Kukol, A., P. D. Adams, L. M. Rice, A. T. Brunger, and T. I. Arkin. 1999. Experimentally based orientational refinement of membrane protein models: a structure for the influenza A M2 H^+ channel. *J. Mol. Biol.* 286:951–962.
19. Torres, J., and I. T. Arkin. 2002. C-deuterated alanine: a new label to study membrane protein structure using site-specific infrared dichroism. *Biophys. J.* 82:1068–1075.
20. Tian, C. L., P. F. Gao, L. H. Pinto, R. A. Lamb, and T. A. Cross. 2003. Initial structural and dynamic characterization of the M2 protein transmembrane and amphipathic helices in lipid bilayers. *Protein Sci.* 12: 2597–2605.
21. Wu, Y. J., and G. A. Voth. 2003. Computational studies of proton transport through the M2 channel. *FEBS Lett.* 552:23–27.
22. Kass, I., and I. T. Arkin. 2005. How pH opens a H^+ channel: The gating mechanism of influenza A M2. *Structure.* 13:1789–1798.
23. Sansom, M. S. P., I. D. Kerr, G. R. Smith, and H. S. Son. 1997. The influenza A virus M2 channel: A molecular modeling and simulation study. *Virology.* 233:163–173.
24. Wu, Y., and G. A. Voth. 2005. A computational study of the closed and open states of the influenza a M2 proton channel. *Biophys. J.* 89:2402–2411.
25. Sakaguchi, T., Q. A. Tu, L. H. Pinto, and R. A. Lamb. 1997. The active oligomeric state of the minimalistic influenza virus M-2 ion channel is a tetramer. *Proc. Natl. Acad. Sci. USA.* 94:5000–5005.
26. Lear, J. D. 2003. Proton conduction through the M2 protein of the influenza A virus; a quantitative, mechanistic analysis of experimental data. *FEBS Lett.* 552:17–22.
27. Smondyrev, A. M., and G. A. Voth. 2002. Molecular dynamics simulation of proton transport through the influenza A virus M2 channel. *Biophys. J.* 83:1987–1996.
28. Wang, C., R. A. Lamb, and L. H. Pinto. 1995. Activation of the M(2) ion-channel of influenza-virus: a role for the transmembrane domain histidine residue. *Biophys. J.* 69:1363–1371.
29. Shimbo, K., D. L. Brassard, R. A. Lamb, and L. H. Pinto. 1996. Ion selectivity and activation of the M(2) ion channel of influenza virus. *Biophys. J.* 70:1335–1346.
30. Wang, C., R. A. Lamb, and L. H. Pinto. 1994. Direct measurement of the influenza A virus M2 protein ion-channel activity in mammalian cells. *Virology.* 205:133–140.
31. Wang, C., K. Takeuchi, L. H. Pinto, and R. A. Lamb. 1993. Ion channel activity of influenza A virus M2 protein: characterization of the amantadine block. *J. Virol.* 67:5585–5594.
32. Lin, T. I., and C. Schroeder. 2001. Definitive assignment of proton selectivity and attoampere unitary current to the M2 ion channel protein of influenza A virus. *Semin. Virol.* 75:3647–3656.
33. Schroeder, C., C. M. Ford, S. A. Wharton, and A. J. Hay. 1994. Functional reconstitution in lipid vesicles of influenza virus M2 protein expressed by baculovirus: evidence for proton-transfer activity. *J. Gen. Virol.* 75:3477–3484.
34. Cao, N. J. Y., W. S. A. Brusilow, J. J. Tomashek, and D. J. Woodbury. 2001. Characterization of reconstituted Fo from wild-type *Escherichia coli* and identification of two other fluxes co-purifying with Fo. *Cell Biochem. Biophys.* 34:305–320.
35. Franklin, M. J., W. S. A. Brusilow, and D. J. Woodbury. 2004. Determination of proton flux and conductance at pH 6.8 through single Fo sectors from *Escherichia coli*. *Biophys. J.* 87:3594–3599.
36. Moffat, J. C., M. D'Haenens, R. Davison, V. Vijayvergiya, D. D. Busath, and D. J. Woodbury. 2004. Measurement of proton flux through influenza A viral protein M2. *Biophys. J.* 86:550a. (Abstr.)
37. Moffat, J. C., M. A. D'Haenens, H. Belnap, V. Vijayvergiya, D. J. Woodbury, and D. D. Busath. 2005. Measurement of proton flux through influenza A viral protein M2 at different pHs. *Biophys. J.* 88:475a. (Abstr.)
38. Rogers, B. L., L. Squires, S. Later, J. C. Moffat, V. Vijayvergiya, F. Gao, and D. D. Busath. 2006. Proton uptake by influenza M2 in proteoliposomes: pH dependence. *Biophys. J.* 90:284a. (Abstr.)
39. Tian, C. L., K. Tobler, R. A. Lamb, L. H. Pinto, and T. A. Cross. 2002. Expression and initial structural insights from solid-state NMR of the M2 proton channel from influenza a virus. *Biochemistry.* 41:11294–11300.
40. Hu, J., R. Fu, K. Nishimura, L. Zhang, H. X. Zhou, D. D. Busath, V. Vijayvergiya, and T. A. Cross. 2006. Histidines, heart of the hydrogen ion channel from influenza A virus: toward an understanding of conductance and proton selectivity. *Proc. Natl. Acad. Sci. USA.* 103: 6865–6870.
41. Betakova, T., F. Ciampor, and A. J. Hay. 2005. Influence of residue 44 on the activity of the M2 proton channel of influenza A virus. *J. Gen. Virol.* 86:181–184.
42. Decoursey, T. E. 2003. Voltage-gated proton channels and other proton transfer pathways. *Physiol. Rev.* 88:475–579.
43. Feniouk, B. A., M. A. Kozlova, D. A. Knorre, D. A. Cherepanov, A. Y. Mulkidjanian, and W. Junge. 2004. The proton-driven rotor of ATP synthase: Ohmic conductance (10 fS), and absence of voltage gating. *Biophys. J.* 86:4094–4109.
44. Decker, E. R., and D. G. Levitt. 1988. Use of weak acids to determine the bulk diffusion limitation of H^+ ion conductance through the gramicidin channel. *Biophys. J.* 53:25–32.
45. Myers, V. B., and D. A. Haydon. 1972. Ion transfer across lipid membranes in the presence of gramicidin A. *Biophys. J.* 274:313–322.
46. Veatch, W. R., E. T. Fossel, and E. R. Blout. 1974. The conformation of gramicidin A. *Biochemistry.* 13:5249–5256.
47. Kochendoerfer, G. G., D. Salom, J. D. Lear, R. Wilk-Orescan, S. B. H. Kent, and W. F. DeGrado. 1999. Total chemical synthesis of the integral membrane protein influenza A virus M2: role of its C-terminal domain in tetramer assembly. *Biochemistry.* 38:11905–11913.